



OPEN Laser-driven proton sources for efficient radiation testing

Beatrice D'Orsi^{1,2}✉, Corrado Altomare³, Alessandro Ampollini⁴, Maria Denise Astorino⁴, Giulia Bazzano⁴, Elias Catrìx¹, Alessia Cemmi², Andrea Colangeli⁴, Ilaria Di Sarcina², Daniele Salvatore Lazzaro³, Ronan Lelièvre^{5,6}, Stefano Loreti⁴, Sylvain Fourmaux¹, Julien Fuchs⁵, Paolo Nenzi⁴, Guglielmo Pagano⁴, Fabio Panza^{4,7}, Concetta Ronsivalle⁴, Jessica Scifo², Simon Vallières¹ & Patrizio Antici¹

Several fields such as particle physics, space exploration, and high-energy physics, use *Commercial Off-The-Shelf* (COTS) electronic components in a high-radiation operative environment. These operating conditions can cause significant damage to electronic circuits, affecting their operational features and thus the reliability of the entire facility. Qualifying and characterizing these components against radiation is essential to ensure their proper functioning in harsh conditions. This study investigates the effect of stress-testing electronic components used in high-radiation environments with various types of radiation sources. The components were exposed to gamma rays, laser-driven protons, conventionally accelerated protons, and neutrons, analyzing the devices parameters after different irradiation conditions. The results indicate significant degradation in electrical performance due to radiation-induced defects and significant variations of the effects at same dose delivery. We show that laser-driven proton irradiation achieves equivalent stress-testing with doses two orders of magnitude lower and much quicker than other radiation sources, demonstrating a much higher stress-testing efficiency.

Keywords Radiation hardness, Transistors, Gamma radiation, Laser-plasma acceleration, Protons, Neutrons, TNSA, TID

Electronic devices are crucial to modern technology but can suffer severe performance degradation due to radiation, especially in applications such as particle and astroparticle physics, space exploration, and high-energy physics. These high-radiation environments can cause significant damage to electronic circuits, affecting their operational features and reliability. Thus, characterizing electronic devices and radiation detectors is essential to ensure their proper functioning in such conditions. Understanding how components behave in radiation environments, including exposure to ionizing radiation and electromagnetic waves, is vital. Electromagnetic waves interacting with semiconductor devices can produce Electromagnetic Pulse (EMP) effects, spanning a broad spectrum from very low frequencies below one hertz to ultrahigh frequencies up to 3 GHz. These interactions can induce harmful current and voltage surges, potentially causing electrical or thermal breakdowns, though these effects are typically temporary, and systems may return to normal operation after the pulse ends^{1,2}. Besides EMPs, electronic devices can also be subjected to ionizing radiation effects. These effects are broadly divided into Single Event Effects (SEEs) and gradual cumulative effects^{3,4}. SEEs occur due to the passage of a single particle depositing energy in the device, potentially causing immediate failures such as memory upsets or burnout. SEEs can happen at any time during the operational period in a radiation environment and may be destructive or non-destructive. In contrast, cumulative damage results from the radiation dose accumulated over the device's lifetime, becoming significant with prolonged exposure. This type of damage is classified into Total Ionizing Dose (TID) effects, which arise from particle/photon energy loss due to ionization, and Displacement Damage (DD) effects, caused by atomic displacement or bulk damage within the material, as a result of Non-Ionizing Energy Loss (NIEL) processes.

¹INRS, EMT Varennes, 1650 Blvd Lionel-Boulet, Varennes J3X 1S2, Canada. ²ENEA Nuclear Department, Via Anguillarese 301, 00123 Rome, Italy. ³IMT Srl, Via Cipriano Faccinetti 67, 00159 Rome, Italy. ⁴ENEA Nuclear Department, Via Enrico Fermi 45, 00044 Frascati (RM), Italy. ⁵LULI, LULI - CNRS, CEA, UPMC Univ Paris 06: Sorbonne Université, Ecole Polytechnique, Institut Polytechnique de Paris, 91128 Palaiseau Cedex, France. ⁶Laboratoire de Micro-Irradiation, de Metrologie et de Dosimetrie des Neutrons, PSE-Sante/SDOS, IRSN, 13115 Saint-Paul-Lez-Durance, France. ⁷INFN – sezione di Genova, via Dodecaneso 33, 16146 Genova, Italy. ✉email: beatrice.dorsi@enea.it

Electronic systems are often used in high radiation environments such as ignition facilities, nuclear plants, space and high luminosity machines^{5–7}. In such hostile environments, there has been a growing interest in Commercial Off-The-Shelf (COTS) components^{8–10}, as they are much cheaper than radiation-hardened and radiation-tolerant alternatives, are readily and easily available, and demonstrate very good electrical performance. However, they are not qualified by the manufacturer for radiation resistance. For this reason, it is essential to qualify these electronic devices before use and to thoroughly understand the radiation effects on them.

Bipolar junction transistors (BJTs), which are commonly made from silicon, are sensitive to both TID and DD^{11,12}. Due to their physical structure and inherent operation, BJTs are more vulnerable to charge accumulation and crystal defect creation under radiation exposure. At the relatively low irradiation energies employed in our experiments, SEEs – including single event latchups, are generally unlikely to occur in bipolar BJTs due to their inherent device structure and current collection mechanisms, which make them less sensitive to the transient disturbances caused by individual radiation events^{13,14}. SEE characterization on BJTs requires specialized testing facilities that are not always readily available, and the particles/photons used in the irradiation tests for this study are not suitable for investigating SEEs¹⁵. For these reasons, this paper focuses on investigating the damage caused by TID and DD effects, without limiting the validity of the results. The NIEL (or DD) dose deposited from gamma, neutron and proton exposure was assessed using sr-niel calculators¹⁶ developed by the Italian Space Agency (ASI) under the ASI Supported Irradiation Facilities (ASIF) program¹⁷.

Recent advances in radiation sources based on laser-driven accelerators, offer compact and time-efficient alternatives to conventional methods¹⁸: by focusing an ultra-intense ($I > 10^{18}$ W/cm²) ultra-short (fs) laser pulse onto a thin foil, ions can be accelerated through laser-plasma interaction^{19,20}, particularly with the Target Normal Sheath Acceleration (TNSA) mechanism²¹. This method can routinely accelerate protons up to tens of MeV^{22,23}, useful for various applications. Current applications for which these particles offer unique prospects include astrophysics^{24,25}, their use as bright ultra-short neutron sources^{26–28}, fusion studies^{29–32}, picosecond metrology³³, an utilization in medicine^{34–36}, as diagnostics in the cultural heritage^{37,38}, for stress testing materials^{18,39} for advanced material synthesis^{40,41}.

While different efforts have been made to stress test materials using laser-accelerated particles and to analyze the generation of strong electromagnetic pulses generated during the interaction, the understanding of the effects of laser-accelerated proton irradiation on electronic components is still outstanding. Here we validate and optimize this stress testing method and compare the results with those from more conventional radiation sources to provide guidelines for using this novel source.

In this paper, COTS BJTs were characterized before and after exposure to various radiation sources, to evaluate their radiation resistance properties in harsh operation environment. Despite MOS technologies being more common for integrated circuits, BJTs remain widely used due to their high performance in amplification and switching applications^{42–45} and provide a solid base for investigations that can easily be transferred. We compared the effects of various radiation sources, including laser-accelerated protons, with conventional sources such as gamma rays, neutrons, and protons accelerated by conventional radio-frequency based accelerators. Our findings indicate that laser-driven protons are characterized by very high dose delivery efficiency, as they induce damage comparable to that of conventional sources in a very short time and delivering less dose, making them a highly effective tool for stress tests. If one would apply a similar reasoning as for radiobiological studies concerning radiobiological effectiveness (RBE)⁴⁶, laser-driven protons have a much higher *stress-testing effectiveness* than other sources.

Pre- and post-irradiation characterizations assessing changes in relevant parameters of BJTs like current gain, leakage currents, saturation voltages, and I_C - V_{CE} characteristics are presented, with particular attention given to the study of current gain, a fundamental parameter for characterizing the performance of BJTs that is most affected by radiation^{12,13,47}. The results obtained from thermal annealing tests conducted to evaluate the potential recovery of the studied parameters, as specified in the ESA standard⁴⁸, are also included (see Supplementary Materials). This analysis is crucial for developing more robust electronic components that maintain reliable operation in high-radiation environments, ensuring the longevity and functionality of future technological advancements, as well as validating and optimizing other innovative stress test sources.

Methods

In order to have a representative device for the testing we focused the investigation on BJTs of the type NPN 2N2222A in a TO-18 package. This choice was driven by the proven reliability, suitable thermal characteristics, and established performance under radiation of this device, making it an optimal choice for our testing objectives. Parametric tests of the BJTs were conducted using a LabVIEW test program in collaboration with the company IMT s.r.l.⁴⁹ that has a wide experience in testing electronic components and in developing advanced systems for different clients in the space industry. A Keysight B2902A Precision Source/Measure Unit was employed to source and measure both current and voltage of the devices under test. The BJTs were characterized before and after irradiation to evaluate changes in their electrical parameters. Specifically, 55 BJTs of the same batch were used. The focus was on the current gain (β) behavior, as the degradation of β is a primary concern regarding the reliability and performance of such devices. The current gain was measured at a fixed collector-emitter voltage (V_{CE}) of 10 V across five different collector current (I_C) values as reported in Table 1.

To assess radiation resistance properties of the devices, the dose values at which the current gains exit nominal specifications provided by datasheets⁵⁰ were determined and chosen as reference to compare different radiation sources.

Additionally, electrical measurements involving leakage currents and saturation voltages evaluation and I_C - V_{CE} curves determination were conducted. The test conditions for cutoff currents and saturation voltages are summarized in Table 2.

Test	Current gain β	Collector current I_C
1	β_1	0.1 mA
2	β_2	1 mA
3	β_3	10 mA
4	β_4	150 mA
5	β_5	500 mA

Table 1. Collector current's test conditions for current gain measurements. The current gain evaluation tests were conducted with a fixed $V_{CE} = 10$ V.

Cutoff currents		Saturation voltages	
I_{CBO1}	$V_{CB} = 75$ V	$V_{CE(sat)1}$	$I_C = 150$ mA, $I_B = 15$ mA
I_{CBO2}	$V_{CB} = 60$ V	$V_{CE(sat)2}$	$I_C = 500$ mA, $I_B = 50$ mA
I_{EBO1}	$V_{EB} = 6$ V	$V_{BE(sat)1}$	$I_C = 150$ mA, $I_B = 15$ mA
I_{EBO2}	$V_{EB} = 4$ V	$V_{BE(sat)2}$	$I_C = 500$ mA, $I_B = 50$ mA
I_{CEO}	$V_{CE} = 50$ V		

Table 2. Test conditions for cutoff currents and saturation voltages measurements.

Irradiation facilities and samples preparation

Gamma irradiation tests were performed at the Calliope gamma irradiation facility equipped with ^{60}Co gamma source (mean energy 1.25 MeV) of the ENEA Casaccia R.C. (Rome, Italy)⁵¹ with a dose rate of 1.1 kGy(Si)/h (dose rate measured in silicon) up to approximately 500 kGy. Gamma exposure was performed in air at room temperature according to ESCC Basic Specification No. 22900. All the samples were biased during irradiation.

Neutron and proton irradiations were conducted at the ENEA Frascati Research Center using the Frascati Neutron Generator (FNG)^{52,53} and the low energy vertical extraction line of the TOP-IMPLART^{54,55} facility, respectively. Specifically, three values of 2.8 MeV (energy spread 0.2 MeV) proton fluences ($3.38 \cdot 10^9$ p/cm², $3.38 \cdot 10^{10}$ p/cm² and $1.3 \cdot 10^{11}$ p/cm²) were used. Regarding neutron irradiation, the tests were conducted with 14 MeV neutrons using different fluences ($2 \cdot 10^9$ n/cm², $2 \cdot 10^{11}$ n/cm², $2 \cdot 10^{12}$ n/cm², $1 \cdot 10^{13}$ n/cm², $2 \cdot 10^{13}$ n/cm²). Neutron and proton irradiation tests were performed in air and all the samples were unbiased during irradiation. To prevent energy loss of protons in the samples lid, the BJTs were decapped for protons irradiation⁵⁶. Before the irradiation test, all samples underwent characterization following the opening procedure.

Laser-driven proton irradiation was carried out at the Advanced Laser Light Source (ALLS) ion beamline of the Institute national de la recherche scientifique (INRS) located in Varennes (Montreal, Canada)⁵⁷ where a 200 TW laser is available enabling laser-driven proton acceleration⁵⁸. The irradiation tests were performed with a varying number of laser shots (1, 5, 50, 100, 250, 400). A typical proton spectrum obtained during the experiment is shown in Fig. 1.

Laser-driven protons irradiation tests were performed in vacuum and all the samples were unbiased during irradiation. As well as for conventional proton irradiation tests, the BJTs were decapped to conduct laser-driven proton irradiation.

Given that the employed radiation sources are heterogeneous, the irradiation conditions are defined using various parameters, namely ^{60}Co deposited dose, number of shots, proton fluence, and neutron fluence. To facilitate comparison of the obtained results, the following section outlines the procedure used to determine the dose delivered by all the employed radiation sources. Specifically, both the NIEL and TID contributions to the deposited dose were considered.

Dose contributions evaluation

Since bulk and surface effects can be regarded as independent of each other, both the dose deposited by ionizing processes and non-ionizing processes were studied for all the radiation sources. Specifically, the sum of these two contributions gives the total deposited dose D^{total} , as follows:

$$D^{\text{total}} = D^{\text{TID}} + D^{\text{NIEL}} \quad (1)$$

where D_{TID} is the dose deposited by ionizing processes, while D^{NIEL} accounts for the dose released after non-ionizing processes.

Gamma radiation deposits energy in matter mainly through ionization processes since ^{60}Co photons (mean energy 1.25 MeV) cannot directly induce displacement damage. However, photons can produce electrons that have sufficient energy (about 260 keV⁵⁹) to induce DD. The dosimetric systems used at the Calliope facility⁵¹ provide the value of the total deposited dose, in this case Electron Spin Resonance (ESR)-alanine dosimeters and Fricke solution were employed. The single contribution of the NIEL dose was obtained through calculations involving the spectrum of Compton electrons generated by the interaction of gamma radiation with the irradiated sample. Specifically, the electron spectrum generated within the sample after exposure was calculated with a Monte Carlo N-Particle® (MCNP®) code⁶⁰ (for details about the simulation, see Supplementary Materials).

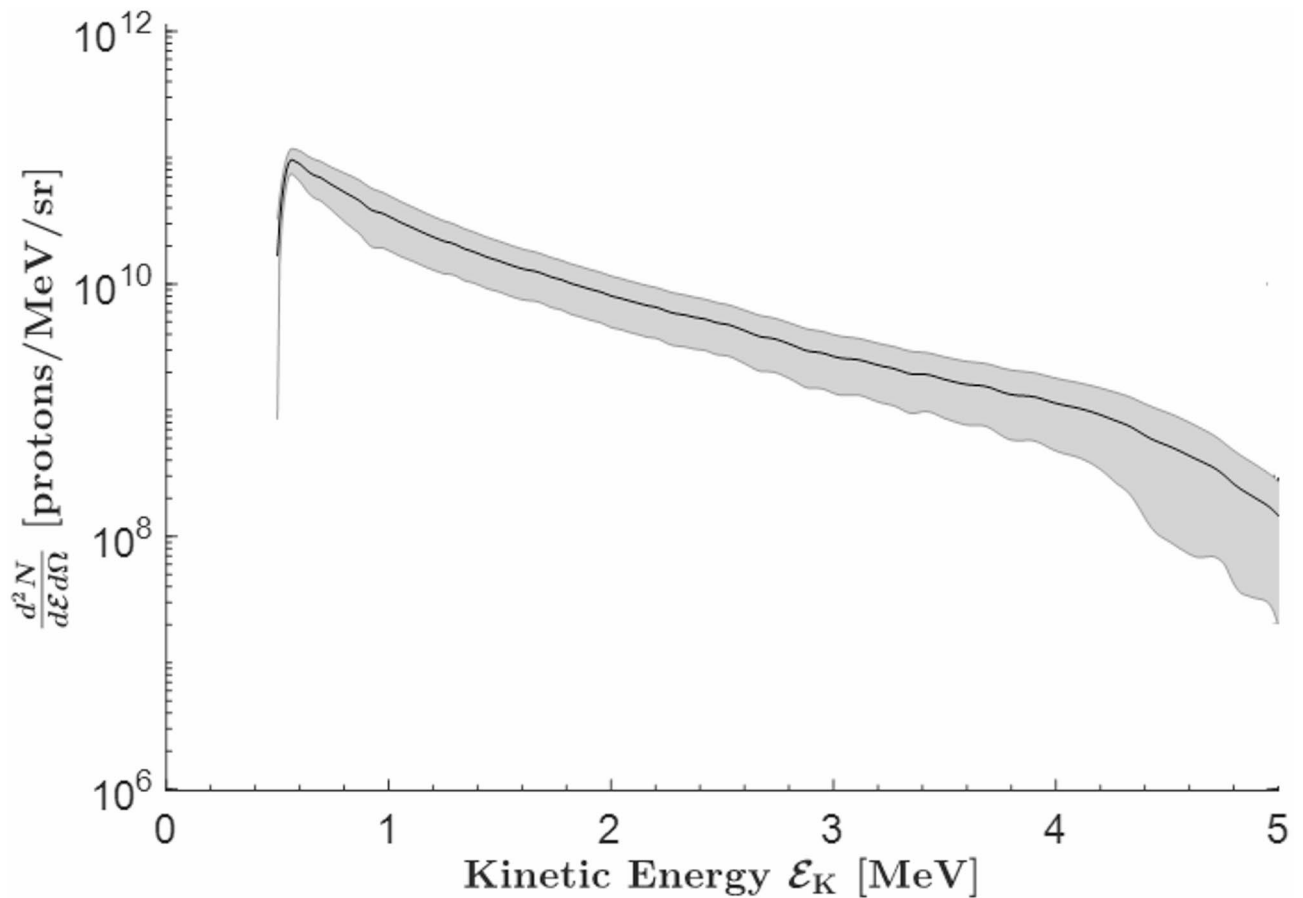


Fig. 1. Routinely available proton spectrum per steradian at the ALLS ion beamline.

Subsequently, the NIEL dose deposited in the sample by electrons was computed using a calculator available on the Italian Space Agency (ASI) website⁶¹. The calculator requires inputs such as particle type, energy spectrum and the target material and gives a NIEL dose value (in Gy). By utilizing the NIEL function¹² of the incident particle, it provides the corresponding NIEL dose. As example, after one hour of gamma irradiation of a BJT, a NIEL dose $D^{\text{NIEL}} \simeq 8 \cdot 10^{-3}$ Gy is deposited within the silicon region of the BJT. The corresponding total absorbed dose D^{total} is 1 kGy.

The total dose deposited by 14 MeV neutrons was obtained by considering the quantity *Kinetic Energy Release in Matter* (KERMA) K expressed in Gray⁶². The kerma coefficient k for 14 MeV neutrons in silicon was obtained from the table reported in⁶³ and therefore, it was possible to obtain the K factors corresponding to different neutron fluences. For example, for a neutron fluence $\Phi_n = 2 \cdot 10^{12}$ n/cm² the kerma factor is $K \simeq 25$ Gy (i.e. $D^{\text{total}} \simeq 25$ Gy). The NIEL deposited dose was obtained with the ASI⁶⁴, using the neutron fluence, neutron energy and sample material. For a neutron fluence of $2 \cdot 10^{12}$ n/cm², it is about $D^{\text{NIEL}} \simeq 1.2$ Gy.

The 2.8 MeV protons produced by the TOP-IMPLART facility are completely absorbed by the silicon layer of the transistor die. Therefore, the total dose (including both ionizing and NIEL contributions) deposited by a given fluence of 2.8 MeV protons was calculated using the dose at the transistor entrance, as given by the following formula:

$$D^{\text{total}} = \left. \frac{dE}{dx} \right|_{2.8 \text{ MeV}} \cdot \Phi_p \cdot 1.6 \cdot 10^{-10} \quad (2)$$

where $\left. \frac{dE}{dx} \right|_{2.8 \text{ MeV}}$ is the stopping power of 2.8 MeV proton in silicon, Φ_p is the proton fluence and $1.6 \cdot 10^{-10}$ accounts for the conversion factor from MeV to Joule to obtain the dose value in Gray. The NIEL deposited dose was computed with the ASI calculator using the proton fluence, the proton energy and the sample material⁶⁵.

To evaluate the dose deposition from protons obtained by a single laser shot, a custom made Matlab® code¹⁸, based on the stopping tables provided by the software SRIM⁶⁶, was used, that had been previously benchmarked with EBT type radiochromic films⁶⁷. The Matlab® code models the energy deposition from a charged particles beam within a sample, resulting in temperature rise. The increase of temperature is related to the absorbed dose in a given volume of the sample by the formula: $D = c_p \Delta T$, where D is the deposited dose, c_p is the sample's material heat capacity and ΔT is the correspondent increase of temperature. The code takes as input the beam parameters (energy and protons number), the distance between the proton source and the sample, and the sample features. Regarding the dose deposited by NIEL processes after a single laser shot, it was obtained using

the ASI calculator⁶⁸, as performed for electrons in the previous section. For a single laser shot, the NIEL dose deposited in the sample is $D_{shot}^{NIEL} = 2.5 \cdot 10^{-3}$ Gy.

The ratios of D^{total} to NIEL dose for the employed radiation sources, as obtained in this section, are summarized in Table 3. This parameter was useful to interpret the results, as will be shown in the following section.

Results and discussion

Radiation resistance properties

As mentioned before, we considered different characteristics of the BJT when looking at its behavior towards stress-testing. We will look firstly, at the I_C - V_{CE} characteristics and then at the current gain for different irradiation methods. BJT characteristics such as cutoff currents and saturation voltages were also analyzed (see Supplementary Materials). They show that these device parameters are only slightly affected by radiation for all radiation methods.

As first radiation source we consider gamma radiation. The I_C - V_{CE} characteristics for all the gamma irradiation conditions at a fixed base current value of $I_B = 50$ μ A (this I_B value ensures that the device operates in a linear region and provides a representative characterization of its response to radiation effects) are shown in Fig. 2a.

One can observe that the values of the I_C vs V_{CE} curves decrease with increasing radiation dose, while the general shape of the I_C behavior as a function of V_{CE} remains unchanged. This indicates a reduction in current amplification, which is further confirmed by the analysis of the current gain, β . After gamma irradiation the current gain shows significant degradation for all the analyzed collector currents (see Fig. 2b). Specifically, the current gains β_1 (measured for the lowest collector current of 0.1 mA) and β_5 (highest collector current, 500 mA) decrease until reaching a constant value after 120 kGy of absorbed dose. For β_2 ($I_C = 1$ mA) the variation in current gain stabilizes after 72 kGy absorbed dose, while β_3 and β_4 decrease after each irradiation step. According to the sample datasheet⁵⁰ that fixes the acceptable ranges for the different current gains, β_1 and β_2 exit the acceptable range after 10 kGy of absorbed dose, β_3 and β_4 after irradiation of approximately 2 kGy and β_5 remains within datasheet's specification until around 100 kGy.

We now look at neutron irradiation. The I_C - V_{CE} curves obtained before and after neutron irradiation remain unchanged until a neutron fluence of $2 \cdot 10^{11}$ n/cm² and then the I_C values decrease with increasing neutron fluence, as shown in Fig. 2c.

The results obtained for the current gains are shown in Fig. 2d. All the β values are unaffected up to a neutron fluence of $2 \cdot 10^{11}$ n/cm², after which they begin to decrease. β_5 remained within specifications even at the highest neutron fluence irradiation condition. However, β_1 and β_2 deviated from the allowed ranges specified by the datasheet after reaching a neutron fluence of approximately $3.5 \cdot 10^{12}$ n/cm², and β_3 and β_4 after reaching a fluence of approximately $2 \cdot 10^{12}$ n/cm². Moreover, it can be observed that experimentally, at low collector currents (< 10 mA) the device's current gain degrades more severely due to the predominance of surface and interface effects. Conversely, at higher collector currents (> 50 mA) performance worsens because bulk damage in the structure becomes dominant. In our case, one can observe that the β_1 and β_2 parameters deteriorate much more rapidly under TID damage than under DD damage—even though no reversal of trend is evident for DD. This aspect will require further in-depth study in future work. It shall be noted that, as reported in the literature, passive mode can still provide informative data on TID effects in bipolar devices^{69,70}.

We compare these results with what was obtained using conventionally accelerated protons. The I_C - V_{CE} characteristic curves before and after irradiation with conventional protons show that the collector current values remain unchanged after proton irradiation with a fluence of $3.38 \cdot 10^9$ p/cm², and then they start to decrease as the proton fluence increases (Fig. 3a).

The results for the current gains are shown in Fig. 3b. The lowest value of proton fluence does not affect the current gain for all conditions of collector currents. After irradiation at $3.38 \cdot 10^{10}$ p/cm², the β values corresponding to collector currents I_C of 0.1 mA, 1 mA, and 10 mA show a decrease, indicating a worsening of the BJT functioning. However, up to this proton fluence, all the β values remain within the acceptable range. After irradiation at $1.3 \cdot 10^{11}$ p/cm², the devices were completely damaged as the current gain values went out of the ranges allowed by the sample datasheet. Finally, we irradiate the samples with laser-accelerated protons. Since every shot produces, within errorbars, the same dose, in some cases we cumulated over several shots to have higher dose depositions, namely over with 1,5 and 50 shots. Based on measurements, and with the adopted configuration, the average dose deposition is 3.5 Gy per shot. After 50 shots the gain values reach their minimum (worst operating point) and cannot be further degraded as tested using 100, 250, and 400 laser shots. From the I_C - V_{CE} characteristic curves before and after irradiation with laser-driven protons, as for the other irradiation sources, a decrease in collector current can be observed with increasing dose (Fig. 3c). Similar conclusions can be drawn from the behavior of current gains after irradiation. Figure 3d depicts the curves corresponding to the current gains β . From Fig. 3d, it is evident that after a few laser shots, the current gain values exit specification limits: specifically, β_3 and β_4 (with a minimum value of 100) goes out of limits after approximately 2 shots, while

	Gamma	Neutrons	Conventional protons	Laser-driven protons
D^{total}/D^{NIEL}	10^5	10^1	10^3	10^3

Table 3. TID and NIEL dose ratios for gamma radiation, neutrons, protons from conventional accelerator and laser-driven protons.

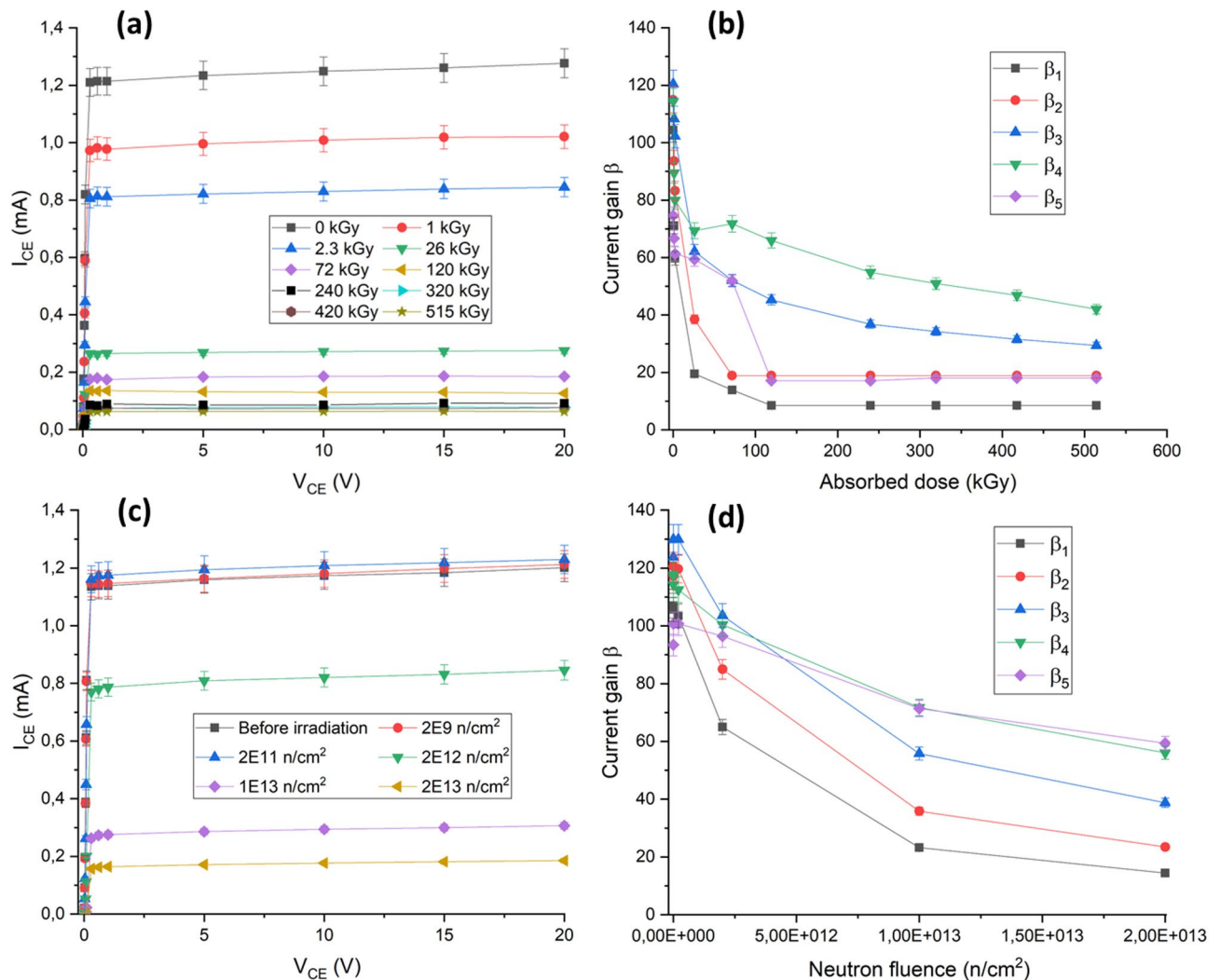


Fig. 2. I_C - V_{CE} characteristic curves of BJTs before and after (a) gamma irradiation at different absorbed dose values and (c) neutron irradiation at different neutron fluence levels. Trends of current gain β as a function of the (b) dose deposited by gamma radiation and d) of neutron fluence measured at $I_C = 0.1, 1, 10, 150, 500$ mA. Error $\Delta(\beta)$: ($\pm 4\%$).

β_1 and β_2 (with minimum values of 50 and 75, respectively) will do so after 3–4 shots. β_5 remains within the allowed range until 5 shots.

All the samples were examined with a Scanning Electron Microscope (SEM) before and after irradiation to detect any morphological changes on the silicon die, but no appreciable modifications were observed (see Supplementary Materials). Hence, we can deduce that the ionizing radiation causes substantial degradation in the electrical performance of BJTs without changes in its morphology. The primary mechanism for this degradation is the introduction of radiation-induced defects at microscopic level which translates in current gain degradation at macroscopic level. In Fig. 4, the scheme of a base-emitter junction of an NPN BJT is shown. Before irradiation, the junction appears as is Fig. 4a. The defects induced by TID and DD dose are shown in Fig. 4b. Specifically, TID induces surface defects, typically at the silicon/silicon oxide (Si/SiO₂) interface (see blue “x” representing interface trapped charges in Fig. 4b) or on the silicon die surface (see the red “+” representing positive oxide trapped charges in Fig. 4b), acting as recombination centers for charge carriers. In contrast, DD dose induces bulk defects: in Fig. 4a, before irradiation, the atoms are ordered (represented by green “X”s), while in Fig. 4b, after irradiation, the disordered “X”s indicate bulk defects, disrupting the atomic structure. This creates interstitial-vacancy pair and/or cluster of defects which harm the functioning of the device.

However, the type and extent of damage varies depending on the radiation source and type of BJT, as will be detailed in the next section.

Dose delivery efficiency

The threshold levels, in terms of D_{total} , D_{TID} and D_{NIEL} calculated according to the procedures described in Section “Dose contributions evaluation”, at which the components functioning is compromised (current gain exit specification), are reported in Table 4. Only the current gain β is considered, rather than the full I_C - V_{CE}

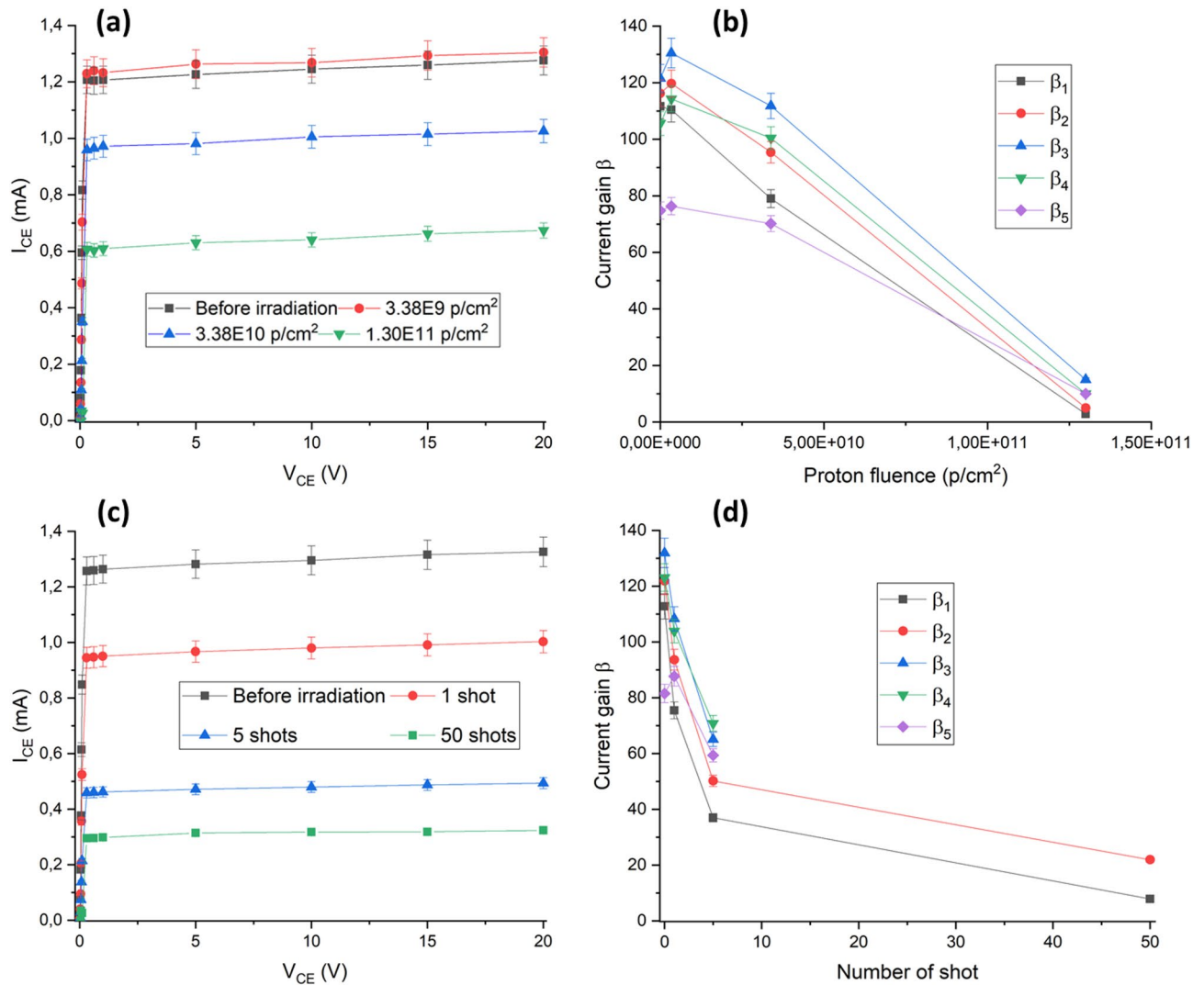


Fig. 3. I_C - V_{CE} characteristic curves of BJTs before and after (a) conventional proton irradiation at different proton fluences and (c) laser-driven proton irradiation at different numbers of shots. Trends of current gain β as a function of the (b) proton fluence and (d) of laser shots measured at $I_C = 0.1, 1, 10, 150, 500$ mA. Error $\Delta(\beta)$: ($\pm 4\%$).

characteristics, because β provides a more direct and quantifiable measure of the transistor performance degradation due to radiation effects. While the I_C - V_{CE} curve provides a detailed view of the transistor behavior over a range of operating conditions, the reduction in β is typically sufficient to indicate the onset of performance loss, as it directly reflects the efficiency of charge carrier amplification and is more sensitive to radiation-induced damage in the transistor. Since β_5 not always exits specifications up to the investigated irradiation conditions, only $\beta_1, \beta_2, \beta_3$ and β_4 are shown.

Among all irradiation methods, gamma radiation requires the highest value of total absorbed dose (up to 8 kGy) to cause the gain value to exit technical datasheet specification, while laser-driven protons require significantly lower doses (up to 13.6 Gy) to achieve similar effects. Conventional protons and neutrons also showed considerable differences in their dose requirements, with neutrons depositing total absorbed dose values approximately two orders of magnitude lower than conventional protons for similar effects on the BJTs. As also indicated in other papers using conventional proton accelerators for stress testing⁷¹, we expect the effect, once a threshold dose has been overcome, to be almost linearly scaling with irradiation dose. As such, within a certain margin, a radiation equivalence can be established between the two irradiation methods. The applicability to other types of electronic components is easily transferable, since they all depend on basic semiconductor technology/components such as found in BJTs.

The observed differences in dose efficiency between ionizing and non-ionizing radiation are primarily due to the distinct mechanisms by which each type of radiation affects semiconductor materials, as well as the different ratios of $D^{\text{total}}/D^{\text{NIEL}}$ (see Table 3). Although the NIEL dose values are much lower than the doses deposited by ionizing radiation processes, the impact of the NIEL dose is far from being negligible and, in certain cases, results in greater damage than the ionizing dose.

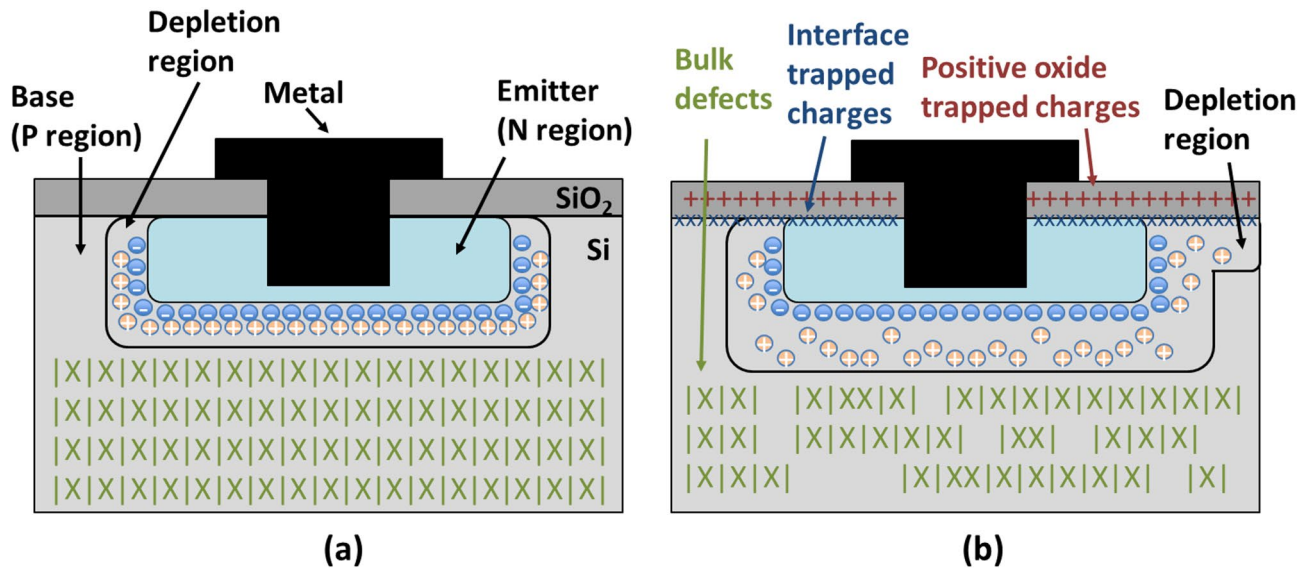


Fig. 4. Simplified scheme of a base emitter junction of a NPN BJT (a) before and (b) after irradiation.

		Gamma	Neutrons	Conventional protons	Laser-driven protons
β_1	D^{total}	8 kGy	62.5 Gy	1.23 kGy	13.6 Gy
	D^{TID}	8 kGy	59.5 Gy	1.23 kGy	13.5 Gy
	D^{NIEL}	0.06 Gy	3.0 Gy	0.28 Gy	0.01 Gy
β_2	D^{total}	7 kGy	43.8 Gy	890 Gy	10.2 Gy
	D^{TID}	7 kGy	41.7 Gy	890 kGy	10.2 Gy
	D^{NIEL}	0.06 Gy	2.1 Gy	0.21 Gy	0.01 Gy
β_3	D^{total}	3 kGy	31.3 Gy	839 Gy	6.8 Gy
	D^{TID}	3 kGy	29.8 Gy	856 Gy	6.8 Gy
	D^{NIEL}	0.02 Gy	1.5 Gy	0.19 Gy	$5.0 \cdot 10^{-3}$ Gy
β_4	D^{total}	600 Gy	25 Gy	685 Gy	6.8 Gy
	D^{TID}	600 Gy	23.8 Gy	685 Gy	6.8 Gy
	D^{NIEL}	$5.0 \cdot 10^{-3}$ Gy	1.2 Gy	0.14 Gy	$5.0 \cdot 10^{-3}$ Gy

Table 4. Values of dose deposited (D^{total} , D^{TID} , and D^{NIEL}) after irradiation with gamma radiation, conventional protons and neutrons, and laser-driven protons, after which the gain values go out of specifications for the previously investigated BJTs. The values error is $\pm 5\%$ and accounts for uncertainties in dose estimation and the extrapolation of dose values.

While TID primarily affects the surface layers of the material, inducing charge accumulation and surface recombination centers, the NIEL dose causes significant disruption within the bulk material of the semiconductor. The NIEL-induced bulk defects, such as point defects, dislocations, and interstitials, disrupt the crystal lattice and impede charge transport. These effects lead to a more pronounced degradation of the device's electrical performance, particularly affecting the current gain β . The correlation between current gain degradation and bulk damage is also supported by the literature⁴⁷. Nonetheless, TID-induced effects at the surface and interfaces should not be underestimated, as the hole yield from primary recombination processes can still play a role, even if it is not the dominant mechanism in the phenomena investigated in this study.

As expected from the literature¹¹, the NIEL contribution to the total absorbed dose due to neutron irradiation is the largest in percentage compared to the other employed radiation sources (Tables 3 and 4: one order of magnitude between NIEL and total dose, while three/four orders of magnitude occur for protons and five for gamma radiation). Consequently, lower total absorbed doses of neutrons are required to cause the same effects on the devices. Conversely, higher total absorbed dose values of gamma radiation are required since the NIEL dose contribution is approximately five orders of magnitude lower than the ionizing one, confirming that high gamma radiation levels are required to cause bulk damage⁷². Looking at the current gain degradation obtained after irradiation of NPN bipolar transistors with laser-driven protons and protons from conventional accelerators, a difference of two orders of magnitude in total absorbed dose is required while both sources had very similar energy ranges (approximately 0.7 MeV to 5 MeV for laser-driven protons and 2.8 MeV with a 0.2 MeV energy spread for TOP-IMPLART protons). Considering the threshold values for β_1 , approximately

$0.7\text{--}10^{11}$ protons, conventionally accelerated, were required to induce comparable damage in the BJT's active region, while approximately $0.8\text{--}10^{11}$ protons, delivered over four laser shots using the ALLS proton spectrum, were needed when using laser-accelerated particles. A significant distinction lies in the total irradiation time and pulse length between laser-driven and conventional proton bunches. The TOP-IMPLART proton beam has a pulse length of about $15\ \mu\text{s}$, delivering approximately 10^7 protons per pulse to the sample's active region. Thus, it required approximately 10^4 pulses over 400 s (with a pulse repetition frequency of 25 Hz) to deliver 10^{11} protons from the TOP-IMPLART source and provide the necessary dose to the sample.

In contrast, the pulse length of the laser-driven protons, considering the samples were positioned at 23.5 cm from the TNSA target and that the protons' velocity depends on their energy, ranging from approximately 0.7 MeV to 5 MeV in this case, was found to be approximately 13 ns. This means that approximately $0.2\text{--}10^{11}$ protons are delivered within tens of nanoseconds when irradiated using laser-driven protons. To perform four shots, given a repetition frequency of 0.65 Hz, approximately 8 s were required, an order of magnitude less.

As such, laser-driven protons are much more efficient regarding dose delivery and can be considered having a higher "stress-testing efficiency" than other radiation sources. This "efficiency" is due to the rapid delivery of protons in a short time frame: laser-driven protons can cause intense mechanical and thermal damage within a very short timeframe, preventing material recovery and potentially leading to device malfunction due to silicon degradation. Similar behavior has already been identified in quick radiation therapy methods, e.g. the FLASH-therapy⁷³, where it has been demonstrated that a short but intense irradiation can be much more efficient than an equivalent dose given over continuous irradiation. Hence, the laser-driven method paves the way for testing and producing more robust electronic components that can withstand the rigors of extreme environments. This will ensure the reliability and longevity of future technological advancements in space, particle physics, and beyond.

Data availability

All data are available in the main text or the supplementary materials, or upon request to the corresponding authors.

Received: 4 February 2025; Accepted: 3 June 2025

Published online: 26 July 2025

References

1. Xi, X. et al. EMP injection damage effects of a bipolar transistor and its relationship between the injecting voltage and energy. *J. Semicond.* **31**, 044005 (2010).
2. Wu, W. B. et al. Combined effects of total ionizing dose and electromagnetic pulse on a bipolar junction transistor. *J. Instrum.* **18**, P04037 (2023).
3. George, J. S. An overview of radiation effects in electronics. In *AIP Conf Proc* Vol. 2160 (2019).
4. Ray, A. Radiation effects and hardening of electronic components and systems: An overview. *Indian J. Phys.* **97**, 3011–3031 (2023).
5. Aguiar, Y. et al. Radiation to electronics impact on CERN LHC operation: Run 2 overview and HL-LHC outlook. In *Proceedings of IPAC2021*, 80–83. <https://doi.org/10.18429/JACOW-IPAC2021-MOPAB013> (2021).
6. Li, Q. et al. Radiation-hard performance research of front-end electronics for fusion diagnostic by Gamma Irradiation Experiment. *Fusion Eng. Des.* **199**, 114160 (2024).
7. Duzellier, S. Radiation effects on electronic devices in space. *Aerosp. Sci. Technol.* **9**, 93–99 (2005).
8. Ferraro, R. et al. COTS optocoupler radiation qualification process for LHC applications based on mixed-field irradiations. *IEEE Trans. Nucl. Sci.* **67**, 1395–1403 (2020).
9. Gutiérrez, O. et al. Toward the use of electronic commercial off-the-shelf devices in space: Assessment of the true radiation environment in low earth orbit (LEO). *Electronics* **12**, 4058 (2023).
10. Budroweit, J. & Patscheider, H. Risk assessment for the use of COTS devices in space systems under consideration of radiation effects. *Electronics* **10**, 1008 (2021).
11. Leroy, C. & Rancoita, P.-G. *Principles of Radiation Interaction in Matter and Detection* (World Scientific, 2016).
12. Leroy, C. & Rancoita, P. G. Particle interaction and displacement damage in silicon devices operated in radiation environments. *Rep. Prog. Phys.* **70**, 493–625 (2007).
13. Assaf, J. Bulk and surface damages in complementary bipolar junction transistors produced by high dose irradiation. *Chin. Phys. B* **27**, 016103 (2018).
14. Li, X. et al. Characteristic of displacement defects in n-p-n transistors caused by various heavy ion irradiations. *IEEE Trans. Nucl. Sci.* **64**, 976–982 (2017).
15. ESA. *Single Event Effects Test Method and Guidelines ESCC Basic Specification No. 25100 - Issue 2*. (2014).
16. Italian Space Agency. Screened Relativistic (SR) Treatment for NIEL Dose Nuclear and Electronic Stopping Power Calculator. <https://www.sr-niel.org/index.php/sr-niel-web-calculators>.
17. Italian Space Agency. ASI Supported Irradiation Facilities: Accordi ASI-ENEA, ASI-INFN.
18. Barberio, M. et al. Laser-accelerated particle beams for stress testing of materials. *Nat. Commun.* **9**, 372 (2018).
19. Afshari, M. et al. Proton acceleration via the TNSA mechanism using a smoothed laser focus. *AIP Adv.* **10**, 35023 (2020).
20. Borghesi, M. Laser-driven ion acceleration: State of the art and emerging mechanisms. *Nucl. Instrum. Methods Phys. Res. A* **740**, 6–9 (2014).
21. Wilks, S. C. et al. Energetic proton generation in ultra-intense laser-solid interactions. *Phys. Plasmas* **8**, 542–549 (2001).
22. Higginson, A. et al. Near-100 MeV protons via a laser-driven transparency-enhanced hybrid acceleration scheme. *Nat. Commun.* **9**, 1–9 (2018).
23. Takagi, Y., Iwata, N., D'Humieres, E. & Sentoku, Y. Multivariate scaling of maximum proton energy in intense laser driven ion acceleration. *Phys. Rev. Res.* **3**, 043140 (2021).
24. Yao, W. et al. Laboratory evidence for proton energization by collisionless shock surfing. *Nat. Phys.* **17**, 1177–1182 (2021).
25. Albertazzi, B. et al. Laboratory formation of a scaled protostellar jet by coaligned poloidal magnetic field. *Science* **1979**(346), 325–328 (2014).
26. Higginson, D. P. et al. Temporal narrowing of neutrons produced by high-intensity short-pulse lasers. *Phys. Rev. Lett.* **115**, 054802 (2015).
27. Roth, M. et al. Bright laser-driven neutron source based on the relativistic transparency of solids. *Phys. Rev. Lett.* **110**, 044802 (2013).
28. Lan, Z. et al. Single-shot laser-driven neutron resonance spectroscopy for temperature profiling. *Nat. Commun.* **15**, 5365 (2024).
29. Patel, P. K. et al. Isochoric heating of solid-density matter with an ultrafast proton beam. *Phys. Rev. Lett.* **91**, 125004 (2003).

30. Malko, S. et al. Proton stopping measurements at low velocity in warm dense carbon. *Nat. Commun.* **13**, 2893 (2022).
31. Rehwald, M. et al. Ultra-short pulse laser acceleration of protons to 80 MeV from cryogenic hydrogen jets tailored to near-critical density. *Nat. Commun.* **14**, 4009 (2023).
32. Sawada, H. et al. Spatiotemporal dynamics of fast electron heating in solid-density matter via XFEL. *Nat. Commun.* **15**, 7528 (2024).
33. Dromey, B. et al. Picosecond metrology of laser-driven proton bursts. *Nat. Commun.* **7**, 10642 (2016).
34. Fuchs, J. et al. Laser-driven proton scaling laws and new paths towards energy increase. *Nat. Phys.* **2**, 48–54 (2005).
35. Robson, L. et al. Scaling of proton acceleration driven by petawatt-laser-plasma interactions. *Nat. Phys.* **3**, 58–62 (2007).
36. Ledingham, K. W. D., Bolton, P. R., Shikazono, N. & Ma, C. M. C. Towards laser driven hadron cancer radiotherapy: A review of progress. *Appl. Sci.* **4**, 402–443 (2014).
37. Barberio, M. & Antici, P. Laser-PIXE using laser-accelerated proton beams. *Sci. Rep.* **9**, 1–9 (2019).
38. Barberio, M., Veltri, S., Scisciò, M. & Antici, P. Laser-accelerated proton beams as diagnostics for cultural heritage. *Sci. Rep.* **7**, 1–8 (2017).
39. Scisciò, M. et al. Analysis of induced stress on materials exposed to laser-plasma radiation during high-intensity laser experiments. *Appl. Surf. Sci.* **421**, 200–204 (2017).
40. Antici, P. et al. Isochoric heating of matter by laser-accelerated high-energy protons. *J. Phys. IV JP* **133**, 1077–1079 (2006).
41. Barberio, M. et al. Laser-generated proton beams for high-precision ultra-fast crystal synthesis. *Sci. Rep.* **7**, 1–9 (2017).
42. Li, X. J. et al. Degradation mechanisms of current gain in NPN transistors. *Chin. Phys. B* **19**, 066103 (2010).
43. You-Run, Z., Bo, Z., Ze-Hong, L., Chang-Jin, L. & Zhao-Ji, L. Thermal analytic model of current gain for bipolar junction transistor-bipolar static induction transistor compound device. *Chin. Phys. B* **18**, 763 (2009).
44. Claeys, C. & Simoen, E. *Radiation Effects in Advanced Semiconductor Materials and Devices* (Springer, 2002).
45. Oo, M. M., Md Rashid, N. K. A., Karim, J. A., Zin, M. R. M. & Hasbullah, N. F. Neutron radiation effect on 2N2222 and NTE 123 NPN silicon bipolar junction transistors. In *IOP Conference Series: Materials Science and Engineering* Vol 53, 012013 (2013).
46. Yogo, A. et al. Measurement of relative biological effectiveness of protons in human cancer cells using a laser-driven quasimonoenergetic proton beamline. *Appl. Phys. Lett.* **98**, 053701 (2011).
47. Consolandi, C. et al. Systematic investigation of monolithic bipolar transistors irradiated with neutrons, heavy ions and electrons for space applications. *Nucl. Instrum. Methods Phys. Res. B* **252**, 276–284 (2006).
48. ESA. *TOTAL DOSE STEADY-STATE IRRADIATION TEST METHOD - ESCC Basic Specification No. 22900*. (2016).
49. IMT. <https://www.imtsrl.it/>.
50. Microsemi. *Technical Data Sheet - NPN Silicon Switching Transistor*.
51. Baccaro, S., Cemmi, A., Di Sarcina, I. & Ferrara, G. Gamma irradiation Calliope facility at ENEA-Casaccia Research Centre (Rome, Italy). *RT/2019/4/ENEA* (2019).
52. Martone, M., Angelone, M. & Pillon, M. The 14 MeV Frascati neutron generator. *J. Nucl. Mater.* **212–215**, 1661–1664 (1994).
53. Pietropaolo, A. et al. The Frascati Neutron Generator: A multipurpose facility for physics and engineering. *J Phys Conf Ser* **1021**, (2018).
54. Nenzi, P. et al. Status of the TOP-IMPLART proton Linac. In *Proceedings of the 31st Int. Linear Accel. Conf.*, 28/08 - 2/09 2022. <https://doi.org/10.18429/JACoW-LINA2022-MOPOGE02> (2022).
55. Piccinini, M. et al. Detection of fluorescent low-energy proton tracks in lithium fluoride crystals. *Radiat. Meas.* **174**, 107140 (2024).
56. ESA. *GUIDELINES FOR DISPLACEMENT DAMAGE IRRADIATION TESTING - ESCC Basic Specification No. 22500*. (2019).
57. ALLS-Beamlines and endstations. <https://alls.inrs.ca/en/>.
58. Catrux, E. et al. Stable high repetition-rate laser-driven proton beam production for multidisciplinary applications on the advanced laser light source ion beamline. *Rev. Sci. Instrum.* **94**, 103003 (2023).
59. Mikeštková, M. et al. The study of gamma-radiation induced displacement damage in n+-in-p silicon diodes. *Nucl. Instrum. Methods Phys. Res. A* **1064**, 169432 (2024).
60. Los Alamos National Laboratory. The MCNP® Code. <https://mcnp.lanl.gov/>.
61. Italian Space Agency. NIEL Dose Calculator for electrons spectral fluence. <https://www.sr-niel.org/index.php/sr-niel-web-calculators/niel-dose-calculator-for-spectral-fluence-of-electrons-protons-and-ions/electrons-niel-dose-calculator>.
62. Thomas, D. J. *ICRU Report 85: Fundamental Quantities and Units for Ionizing Radiation. Radiation Protection Dosimetry* Vol. 150 (Oxford Academic, 2012).
63. Caswell, R. S., Coyne, J. J. & Randolph, M. L. Kerma factors of elements and compounds for neutron energies below 30 MeV. *Int. J. Appl. Radiat. Isot.* **33**, 1227–1262 (1982).
64. Italian Space Agency. Neutrons NIEL Calculator Using ASTM Standards. <https://www.sr-niel.org/index.php/sr-niel-web-calculators/niel-calculator-for-neutrons-using-astm-standards/neutrons-niel-calculator>.
65. Italian Space Agency. Protons & Ions NIEL Calculator. <https://www.sr-niel.org/index.php/sr-niel-web-calculators/niel-calculator-for-electrons-protons-and-ions/protons-ions-niel-calculator>.
66. Ziegler, J. F., Ziegler, M. D. & Biersack, J. P. SRIM—The stopping and range of ions in matter (2010). *Nucl. Instrum. Methods Phys. Res. B* **268**, 1818–1823 (2010).
67. Vallières, S. et al. Low-energy proton calibration and energy-dependence linearization of EBT-XD radiochromic films. *Rev. Sci. Instrum.* **90**, 083301 (2019).
68. Italian Space Agency. NIEL Dose Calculator Protons & Ions spectral fluence. <https://www.sr-niel.org/index.php/sr-niel-web-calculators/niel-dose-calculator-for-spectral-fluence-of-electrons-protons-and-ions/protons-ions-niel-dose-calculator>.
69. Petrov, A. S. & Ulimov, V. N. Some features of degradation in bipolar transistors at different test conditions for total ionizing dose effect. *Microelectron. Reliab.* **52**, 2435–2437 (2012).
70. Dj Vukić, V., Vukić, V. & Osmokrović, P. Total ionizing dose degradation of power bipolar integrated circuit. *J. Optoelectron. Adv. Mater.* **10**, 219–228 (2008).
71. Li, X., Liu, C. & Yang, J. Synergistic effect of ionization and displacement damage in NPN transistors caused by protons with various energies. *IEEE Trans. Nucl. Sci.* **62**, 1375–1382 (2015).
72. Vavilov, V. S. & Ukhin, N. A. *Radiation Effects in Semiconductors and Semiconductor Devices* (Springer, 1995).
73. Montay-Gruel, P., Corde, S., Laissue, J. A. & Bazalova-Carter, M. FLASH radiotherapy with photon beams. *Med. Phys.* **49**, 2055–2067 (2022).

Acknowledgements

The authors would like to acknowledge the staff of the ALLS facility: Joël Maltais for their technical assistance during the experiment. The authors also wish to express their gratitude to the Calliope research group (ENEA NUC-IRAD-GAM), as well as the staff of ENEA NUC-TECFIS-ACP and ENEA NUC-FUSEN-TEN for their support and availability during the experiments. Additionally, we would like to thank the staff of IMT srl for providing the instrumentation for the electrical measurements. We would also like to thank Daniele Mirabile Gattia and Catalin Harnagea for their help with SEM measurements at ENEA and INRS, respectively.

Author contributions

Conceptualization: P.A., B.D.; Methodology: B.D., C.A., D.S.L., G.P., A.A., P.N.; Investigation: B.D., C.A., A.A., M.D.A., G.B., E.C., A.Ce., A.Co., S.L., R.L., S.L., S.F., P.N., G.P., F.P., C.R., J.S., S.V.; Visualization: B.D.; Supervision: J.F., I.D.S., A.Ce., P.A.; Writing—original draft: B.D., P.A.; Writing—review & editing: B.D., P.A. with the help of all authors.

Competing interests

The authors declare no competing interests.

Additional information

Supplementary Information The online version contains supplementary material available at <https://doi.org/10.1038/s41598-025-05682-x>.

Correspondence and requests for materials should be addressed to B.D.

Reprints and permissions information is available at www.nature.com/reprints.

Publisher's note Springer Nature remains neutral with regard to jurisdictional claims in published maps and institutional affiliations.

Open Access This article is licensed under a Creative Commons Attribution-NonCommercial-NoDerivatives 4.0 International License, which permits any non-commercial use, sharing, distribution and reproduction in any medium or format, as long as you give appropriate credit to the original author(s) and the source, provide a link to the Creative Commons licence, and indicate if you modified the licensed material. You do not have permission under this licence to share adapted material derived from this article or parts of it. The images or other third party material in this article are included in the article's Creative Commons licence, unless indicated otherwise in a credit line to the material. If material is not included in the article's Creative Commons licence and your intended use is not permitted by statutory regulation or exceeds the permitted use, you will need to obtain permission directly from the copyright holder. To view a copy of this licence, visit <http://creativecommons.org/licenses/by-nc-nd/4.0/>.

© The Author(s) 2025